

Hydrogen interactions with cavities in helium-implanted silicon

S. M. Myers, D. M. Follstaedt, H. J. Stein, and W. R. Wampler

Sandia National Laboratories, Albuquerque, New Mexico 87185

(Received 16 November 1992; revised manuscript received 28 January 1993)

Hydrogen interactions with microscopic cavities in Si were quantitatively characterized in thermal-release experiments. Closed internal cavities were formed by He-ion implantation and annealing and were characterized by transmission-electron microscopy. The isotopes protium (^1H) and deuterium (D) were introduced by ion implantation or heating in H_2 gas. During temperature ramping the redistribution and release of D were monitored by nuclear-reaction profiling, and the bonding of ^1H was selectively examined by infrared absorption spectroscopy. By exploiting the properties of closed internal surfaces this study determined the Si-H bond energy for surface monohydrides, the result being 2.5 ± 0.2 eV. Hydrogen bonded to the internal surfaces was found to lie several tenths of an eV lower in energy than H_2 gas and H trapped at lattice defects. The oxidized external surface of the Si specimens did not detectably impede H release, implying an efficient recombination process at the Si-SiO₂ interface for which possible mechanisms are considered.

I. INTRODUCTION

Hydrogen reacts strongly with dangling bonds on Si surfaces, and this has a number of consequences for the synthesis and properties of semiconductor structures. For example, H termination on HF-etched Si surfaces provides beneficial chemical passivation,¹ and similar effects have been reported following treatment with H plasmas.² In the photoluminescence of anodized porous Si (Ref. 3), H surface states have been reported to be necessary for the luminescence to occur;⁴ moreover, some investigators have proposed that surface H states are directly responsible for light emission rather than simply providing passivation of carrier-recombination centers.⁵ Hydrogenated gaseous species such as silane and germane are widely used in H_2 carrier gas for chemical-vapor deposition of epitaxial semiconductor layers, and in such processing the H inhibits growth by competing for reactive sites.⁶ Further, when epitaxial growth is carried out at lower temperatures using molecular beam epitaxy, it has proved necessary to first desorb H already present on the surface.⁷

The above considerations and the underlying scientific issues have stimulated extensive and successful efforts to characterize H interactions at external (100) and (111) surfaces on Si. Structural information from scanning tunneling microscopy (STM) and low-energy electron diffraction (LEED) (Refs. 8–10, and citations therein) has been accompanied by infrared (IR) vibrational spectroscopy of the various Si-H bonds.^{1,11–13} In addition, thermal-desorption experiments have illuminated the kinetics and energetics of the surface reactions.^{14–19} Significant gaps in knowledge remain, however, and one of the most important is the strength of the Si-H surface bond. As we shall discuss, this deficiency results from an inherent indeterminacy in the interpretation of the measured activation energy for H_2 thermal desorption. Also not fully resolved are the specific reaction paths by which molecular H_2 is adsorbed and desorbed on Si.

In the present investigation we examined thermal release of H that was bound to *closed internal* surfaces within Si. Helium ion implantation and subsequent annealing produced cavities with a typical diameter of 10 nm as observed by transmission electron microscopy (TEM), with the He being outgassed during the heat treatment. (Similar He-implanted microstructures in Si were reported by Griffioen *et al.*²⁰) Hydrogen was introduced by ion implantation or heating in H_2 gas, and the reaction with Si dangling bonds was detected using IR spectroscopy. Thermal H release was induced by temperature ramping, and the retained quantity was monitored as a function of temperature by nuclear-reaction analysis. By thus examining H reactions at internal rather than external surfaces, it was possible for the first time to determine quantitatively the strength of the Si-H surface monohydride bond.

The Si-H bond-dissociation energy obtained in the present paper is 2.5 ± 0.2 eV. This value is close to the one previously found for Si-H bonding at the Si side of the Si-SiO₂ interface, 2.56 ± 0.06 eV,²¹ but it is substantially smaller than that reported for the $\text{H}_3\text{Si-H}$ bond in silane, 3.9 eV.²² This difference will be discussed in light of recent theoretical results on Si-H bonding.^{23,24} We will also briefly consider implications of this surface-bond energy for the reaction paths and rates of H_2 desorption and adsorption on Si.

The present experiments also illuminate other aspects of H behavior in Si. Because the specimens contained displacement damage and internal open volume as well as internal surfaces, with all of these entities being well removed from the external surface, it was possible to evaluate the relative strengths of the binding of H at lattice defects, in H_2 gas, and on surfaces. Furthermore, the fact that our experiments exhibited no H-barrier effects at the oxidized external surface of the Si has implications for the mechanism of H movement between Si and SiO₂.

In addition to the work reported here, our investigation of H interactions at internal Si surfaces has included

detailed IR spectroscopic studies²⁵ and nuclear-reaction measurements of thermodynamic equilibrium between external H₂ gas and internal-surface Si-H states.²⁶ Preliminary results of the present experiments were reported elsewhere.²⁷

II. BACKGROUND AND APPROACH

A. Hydrogen surface states on cavity walls

In this paper we are concerned with the most strongly bound surface states of the H, namely the monohydrides, for which no more than one H atom is bonded to any surface Si atom. Consequently, the less stable dihydride and trihydride states will not be considered here. On the (100) surface the monohydride forms without disruption of the 2×1 reconstruction, H atoms being attached to the single dangling bond that remains on each surface atom after Si-Si dimerization.⁸ In the case of the (111) surface, an ideally terminated 1×1 configuration has been reported where each Si surface atom is tetrahedrally bonded to three underlying Si atoms and to one H atom located directly above.¹ The situation is more complicated in the presence of the (111) 7×7 reconstruction. Here, Si “rest atoms,” whose bonding is like that of the unreconstructed surface, are accompanied by Si “adatoms;” the latter form bonds with three former rest atoms, thereby replacing three rest-atom dangling bonds with a single, inequivalent, adatom dangling bond.⁹ Hence the reconstructed (111) surface has at least two types of binding sites for H, and this presents a potential complication in the present work. Experimental and theoretical studies of Ge surfaces, however, indicated that H has less affinity for adatoms than for rest atoms due to a transfer of charge from the former to the latter; the calculated energy difference is about 0.7 eV for Ge.²⁸ Consequently, while adatoms may have occurred on the internal surfaces of the present study, their presence is not expected to be important for our interpretation of thermal release from the most strongly bound H states.

With the above as background, we now consider the extent to which the bonding of H at internal cavity walls in Si can serve to illuminate binding energies for ideal (100) and (111) surfaces. As will be seen, our room-temperature He ion implantations followed by heating at 973 or 1073 K produced cavities with diameters near 10 nm. The heat treatments were sufficient to induce thermal release of most of the implanted He, to anneal displacement damage, and to produce (100) and (111) faceting of the cavity walls, so that relatively stable surface configuration of the Si atoms should have been achieved. We therefore believe that most of the dangling bonds on the cavity walls resided on Si atoms which were bonded to three other Si atoms, as opposed to one or two Si atoms where the configurational energy would be much larger. As will be seen, this view is supported by IR vibrational spectra of the Si-H bonds forming on the cavity walls. There is uncertainty, however, regarding longer-range order on the cavity walls. In particular, while the simple 2×1 reconstruction appears likely on the (100) facets, we cannot predict the extent and type of

reconstruction on the (111) surfaces. Moreover, the cavities also exhibit curved surfaces, and for such regions the character of the longer-range order is even less known.

The above considerations indicate that the immediate environment of the Si-H monohydride bond on the cavity walls should be very similar to that for ideal surfaces. Specifically, in both cases a single H atom is bonded to a Si atom which is also bonded to three other Si atoms, with the Si-H bond protruding unobstructed into a void. These factors are believed to be the dominant ones in determining the Si-H bond energy, with longer-range order having less influence. We therefore argue that the bond energy obtained herein should be close to that for ideal surfaces. Moreover, the bonding of H on ideal surfaces should be represented much better by cavity walls than by the silane molecule, where the Si atom has four Si-H bonds instead of one.

B. The Si-H bond energy and its relation to H₂ adsorption and desorption

Thermal desorption of H₂ from monohydride states on external (100) and (111) Si surfaces has been measured by several groups. The derived activation energies E_D are fairly consistent and are quite similar for the two orientations. In the case of the (100) surface, values of 2.0 and 2.5 eV were reported;^{17,18} in porous Si where IR vibrational spectroscopy indicated Si-H bonding similar to that on the (100) surface, the result was $E_D = 2.8$ eV;¹⁶ for the (111) surface, activation energies of 2.5, 2.6, 2.7, and 2.4 eV were obtained.^{14,15,18,19} For purposes of the present discussion we will use the average value of $E_D = 2.5$ eV.

The relationship between the Si-H bond energy E_B and the measured activation energy for H₂ desorption E_D has an inherent indeterminacy which has been recognized by previous investigators. It arises because the molecular desorption involves not only the breaking of two Si-H bonds but also formation of the H-H bond with recombination energy $E_R = 4.52$ eV. In one limiting scenario that is reminiscent of metal surfaces, the breaking of two Si-H bonds and H₂ formation are concurrent, and E_D is equal to the energy difference between the final and initial states, $2E_B - E_R$. At the opposite extreme, one can envision disruption of one Si-H bond followed by the exothermic reaction $H + Si-H \rightarrow H_2 + Si-$, where Si- represents the surface dangling bond. Under this condition E_D might approach E_B . We thus arrive at a general relation containing a reaction-path-dependent quantity E_A :

$$E_D = 2E_B - E_R + E_A, \quad 0 \leq E_A \lesssim E_R - E_B. \quad (1)$$

The interdependence of the four energies in Eq. (1) is seen graphically in Fig. 1, which schematically depicts H₂ desorption from Si and also the reverse process of H₂ chemisorption. It is apparent that the parameter E_A is equal to the activation energy for dissociative H₂ adsorption. The energies in the equation include any effects of reconstruction occurring during the reaction.

In the absence of direct measurements of E_B , its value

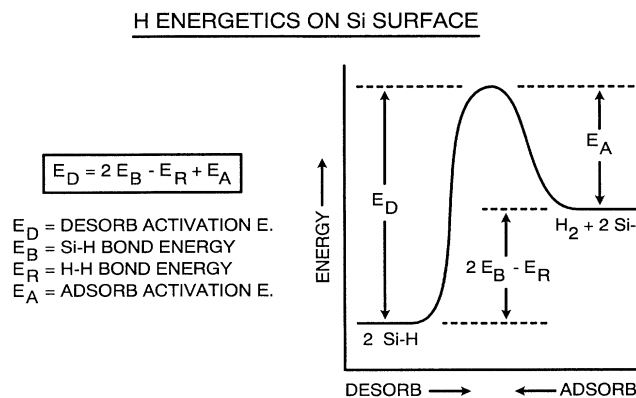


FIG. 1. Energy relationships affecting H_2 desorption and adsorption on Si.

has often been assumed comparable to the dissociation energy for the H_3Si-H bond in silane, about 3.9 eV.²² While this is plausible, the large resulting value leads to difficulties in interpreting experimental observations. For example, if the representative value $E_D = 2.5$ eV is used in Eq. (1), then E_A decreases to zero as E_B increases to 3.5 eV, with larger values of E_B giving unphysical results. Hence, there should be little if any activation barrier for dissociative adsorption of H_2 on the Si surface. This appears inconsistent with the generally observed difficulty of chemisorbing H on Si from H_2 gas, which has compelled investigators to use atomic H or to employ HF acid etching. (See, e.g., Refs. 8 and 1.)

A second difficulty for large E_B values arises from recent electron-paramagnetic-resonance (EPR) experiments, which measured the activation energy for dissociation of the Si-H bond at the Si side of the (111) Si-SiO₂ interface.²¹ The local environment of the interfacial bond is similar to that of Si-H at rest atoms on the (111) Si surface; in particular, at the interface, (1) the Si-H pair is oriented perpendicular to the surface, (2) the Si atom is tetrahedrally bonded to three underlying atoms of the Si crystal, (3) Si-O bonds occur only at next-nearest-neighbor Si sites, and (4) the overlying glassy Si-O network is believed to be open and unreactive. The interface environment has the important simplifying property, however, that the Si-H bonds are widely separated, so that H-H recombination cannot be concurrent with breaking of the Si-H bond. Hence, in contrast to the situation on the Si surface, the measured activation energy can be unambiguously equated to the Si-H bond-dissociation energy. The value obtained in the EPR experiments was 2.56 ± 0.06 eV, or more than 1 eV smaller than the bond energy in silane.

C. Thermal release of hydrogen from internal surfaces

Because the present experiments measured thermal H release from internal rather than external surfaces of Si, it was possible to obtain further information on the energetics of Fig. 1. The key difference between the two approaches lies in the reaction path going from surface Si-H to external H_2 gas. In the case of the internal surfaces,

external desorption is preceded by promotion of H atoms from the bound internal-surface state into solid solution and then by H diffusion to the external surface. We will argue on the basis of experimental evidence that the single-H processes of promotion and diffusion are rate determining, so that the inherent indeterminacy in the relationship between the Si-H bond strength and the desorption activation energy is circumvented. The measured thermal release is instead sensitive to the Si-H bond energy, the solution energy, and the diffusion activation energy, and since the latter two quantities are independently known,²⁹ the Si-H bond strength E_B can be extracted. Then, with E_D being taken from the experiments on external-surface desorption, the energetics depicted in Fig. 1 are fully determined.

D. Diffusion-trapping mathematical formalism

In order to extract the Si-H surface-bond energy from temperature-ramp data it was necessary to employ a mathematical treatment of the trapping, diffusion, and surface-desorption processes. As will be seen in Sec. IV, the behavior of the H during its release from the internal surfaces above 900 K was relatively simple, with a single type of microstructurally stable trap being dominant and no significant barrier effects occurring at the external surface. This condition would allow the use of a correspondingly simple kinetic model to obtain E_B . We also wished to examine other issues, however, including the weaker binding of H to defect traps, the formation of H_2 gas within the cavities, the influence of hypothetical permeation barriers at the oxidized Si surface, and the degree to which He was retained within the cavities after post-implantation annealing. Therefore, in the present subsection we first present a more general treatment that encompasses all of these effects and will actually be used for data analysis. Then, to provide physical insight, we indicate the considerable simplifications that arise for the high-temperature release of H from the internal surfaces.

In these calculations, untrapped H in lattice solution will be treated as dissociated atoms having a unique diffusion coefficient and a well-defined solid solubility with the expected square-root dependence on H_2 pressure. This description has been validated at temperatures above 1365 K by detailed diffusion and solubility measurements.²⁹ Moreover, the permeability, equal to the product of the diffusivity and solubility, has been measured at 873 K, and the value conforms quantitatively to an Arrhenius extrapolation of the higher-temperature data.³⁰ Hence, the straightforward treatment of solution behavior appears justified for the temperatures of H release in the present studies.

The transport equations for H in the presence of static traps and external-surface permeation barriers, together with numerical methods of solution, have been discussed in detail elsewhere.³¹ Here we summarize the relevant equations and indicate extensions necessary to describe H_2 and He gases within internal cavities. For the atomic fraction of mobile H in solution, C_s , one has

$$[\partial/\partial t]C_s(x,t) = D_s[\partial^2/\partial x^2]C_s(x,t) - \Sigma_i S_i(x,t), \quad (2)$$

where D_s is the diffusion coefficient of H in solution, and the terms S_i describe the exchange of H between solution and traps of type i . The atomic fractions of trapped H, C_i , are given by

$$[\partial/\partial t]C_i(x,t) = S_i(x,t). \quad (3)$$

For static traps that present no activation barriers to H attachment, S_i can be expressed as

$$S_i(x,t) = 4\pi N_h D_s [R_i/n_i] \{ C_s(x,t) [A_i(x) - C_i(x,t)] - C_i \exp(-Q_i/kT) \}. \quad (4)$$

In Eq. (4), N_h is the atomic density of the host matrix; R_i is the capture radius for a discrete trapping entity such as a cavity; n_i is the number of H attachment sites per trapping entity, being for a cavity the number of dangling bonds on the wall; A_i is the atomic fraction of attachment sites for H; and Q_i is the positive binding energy per H atom at the trap site expressed relative to H in solution. The nonconfigurational part of the entropy difference between solution and sinks has been neglected. The physical meaning of Eq. (4) is illuminated by considering the following two limiting cases: first, when $C_i = 0$ so that there is no detrapping, S_i reduces to the rate for diffusion-limited flow to spherical sinks;³² and, second, when $S_i = 0$ corresponding to an unchanging trap occupancy, the resulting null of the expression within braces describes local thermodynamic equilibrium between solution and traps. In the general case, Eq. (4) describes continuous evolution toward local thermodynamic equilibrium between solution and traps at a rate that is diffusion controlled.

In the above formalism we use the index number $i = 3$ to designate cavity-well traps, these being the strongest of three H traps to be considered in the present paper. The trap binding energy Q_3 is simply related to the desired Si-H bond energy on the Si surface, E_B ; the two quantities differ only in their reference states, which are, respectively, atomic H in solid solution and atomic H in vacuum. Hence,

$$E_B = Q_3 - E_S + E_R/2, \quad (5)$$

where $E_S = 1.86$ eV is the well-established energy per atom required to promote H from molecular gas to solution in Si (Ref. 29) and $E_R = 4.52$ eV is the dissociation energy of H_2 . The relationships among the four energies in Eq. (5) are depicted schematically in Fig. 2.

We now move beyond Ref. 31 to consider the modification of Eq. (4) which is necessary to treat the behavior of molecular gas, either H_2 or He, within the cavity open volumes. This capability will not be used to extract binding energies, which is our primary objective, but it is needed to assess semiquantitatively the extents of H_2 formation and He retention. We assume continuous equilibrium between the gas phase contained in any cavity and the *immediately adjoining* wall sites and lattice-solution sites, so that the approach to local equilibrium between cavities and solution at a particular depth is diffusion limited in the manner of Eq. (4). In the case of H, continuous gas-wall equilibrium requires sufficiently

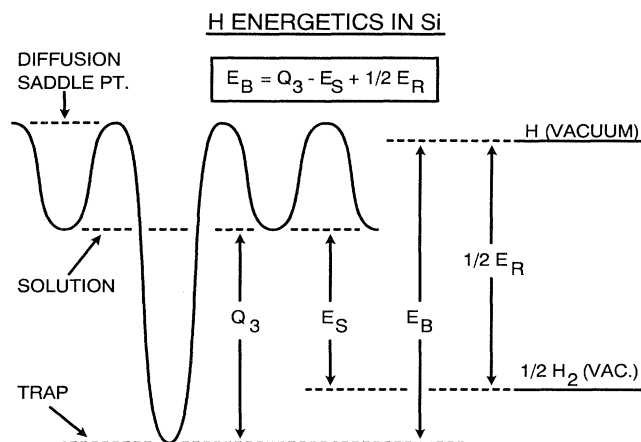


FIG. 2. Energetics of H in Si and in vacuum.

rapid recombinative desorption of H_2 into the cavity balanced by dissociative adsorption from the accumulated gas. Estimates utilizing previous measurements of external-surface desorption¹⁸ indicate that the assumption is justified for the present experiments.

Since the equilibrium between solid solution and molecular gas is different from that between solution and static lattice traps, a corresponding change is required in the expression within braces in Eq. (4). In the case of a diatomic gas such as H_2 one has

$$S_i(x,t) = 4\pi N_h D_s [R_i/n_i] A_i(x) \times \{ C_s(x,t) - C_{so} [F_i(C_i, A_i, T)]^{1/2} \times \exp(-Q_i/kT) \} \quad (6)$$

where C_{so} is the solubility prefactor, F_i is the fugacity of the gas within the cavity, and Q_i is the solubility activation energy. (The fugacity is related to the molecular chemical potential μ by $F = F_0 \exp(\mu/kT)$ with the constant F_0 being such that F reduces to pressure for an ideal gas. See, e.g., Ref. 33.) When the encapsulated gas is monatomic, as for He, the fugacity factor $F^{1/2}$ is replaced by F .

For the purposes of the present paper it was not necessary to treat the difference between fugacity and pressure precisely, but we found it useful to include the effects of nonideality at a semiquantitative level. To this end we added the Van der Waals volume term to the gas equation of state but neglected the attractive term, which is small for H_2 and He; this gives $P(v-b) = kT$, where P is the pressure and b is the Van der Waals molecular volume. It can be shown that the fugacity then is given by $F = [kT/(v-b)] \exp[b/(v-b)]$. Notational compatibility with Eq. (6) was achieved by defining the number of H sites per cavity, n_i , and the atomic fraction of available H sites, A_i , so that these quantities reflect the amount of H given by the gas equation of state when $P \rightarrow \infty$. With this stipulation one has

$$n_i = (4/3)\pi(R_i)^3 n_m / b,$$

$$A_i = V_c n_m / (N_h b),$$

and

$$F_i(C_i, A_i, T) = [kT/b][C_i/(A_i - C_i)] \times \exp[C_i/(A_i - C_i)], \quad (7)$$

where n_m and V_c are the number of atoms per molecule and the cavity volume fraction, respectively.

The remaining aspect of the general formalism to be discussed is the boundary condition on C_s at the external surface of the sample. All fitting of experimental data was done using the condition $C_s(x \rightarrow 0, t) = 0$, corresponding to uninhibited surface release. Additional calculations were performed to explore the effects of hypothetical surface barriers, however, and here we treated the surface release in two steps: first, the fractional population of surface sites, Θ , was taken to be in equilibrium with the adjacent lattice solution, so that $\Theta(t)/[1 - \Theta] = C_s(x \rightarrow 0, t) \exp(Q_\Theta/kT)$, where Q_Θ is the positive energy difference between H in solution and H on the surface; then, the number of H atoms lost per unit area and time was given by $[\partial/\partial t]\Lambda_H = -K_\Theta(T)\Theta^\alpha$, where Λ_H is the depth-integrated areal density of H within the sample, K_Θ is a temperature-dependent rate coefficient, and α is the order of the desorption reaction.

We now return to the trapping formalism of Eqs. (2)–(5). In order to convey the properties and physical meaning of these equations, it is useful to discuss the considerable simplifications that result from a set of approximations that are, in fact, quite accurate for the high-temperature release of H from internal surfaces. The approximations are as follows.

(1) The behavior of the system is dominated by a single type of trap.

(2) At any given depth there is local equilibrium between H in solution and trapped H, so that the expression in braces on the right-hand side of Eq. (4) equals zero. (This condition is well satisfied at temperatures of appreciable H release if the number of diffusive jumps between the trap and the external surface is much larger than one and if the energy saddle point adjacent to the trap is not significantly higher than other diffusion saddle points.)

(3) All of the traps are located at the same depth, $x = l$.

(4) The amount of H in solution is much smaller than that in traps, and as a consequence most of the H migrates to the surface under a steady-state diffusion profile.

(5) There is no barrier to H release at the external surface. Under these conditions Eqs. (2)–(4) yield the following equation for the depth-integrated areal density of retained H, Λ_H , in terms of the areal density of trap sites, Λ_T , and the trap binding energy Q_T :

$$[d/dt]\Lambda_H = -[N_h D_s / l] \{ \Lambda_H / [\Lambda_T - \Lambda_H] \} \exp(-Q_T/kT). \quad (8)$$

When D_s is taken from the literature and Λ_T is determined experimentally by deliberate saturation, Q_T can be obtained by fitting to experimental release measurements, and the desired bond energy E_B is then given by Eq. (5).

III. EXPERIMENTAL PROCEDURE

Samples with a polished (111) face and dimensions of $12 \times 12 \times 0.25 \text{ mm}^3$ were prepared from high-purity Si having a room-temperature resistivity of $2 \text{ k}\Omega \text{ cm}$. Cavity formation was initiated in a near-surface layer by ^4He ion implantation at room temperature, 30-keV energy, and a fluence of 1000 nm^{-2} . In several instances a second implantation was performed using 700-keV ^3He at the same fluence to produce an additional, deeper cavity layer. The resulting He depth distributions, as predicted using the TRIM-90 Monte Carlo range code,³⁴ are shown in Fig. 3. One of the specimens was implanted with Si^+ ions instead of He to simulate the effects of the He displacement damage without forming bubbles; this treatment was performed at 200 keV and a fluence of 90 Si/nm^2 , parameters chosen on the basis of TRIM simulations. Additionally, one sample received no implantation treatment apart from the D injection to be discussed below. The specimens were then annealed for 30 min at 973 K or for 1 h at 1073 K in an ion-pumped vacuum of approximately $3 \times 10^{-5} \text{ Pa}$ ($2 \times 10^{-7} \text{ Torr}$) to enlarge the bubble cavities, to induce outgassing of the He, and to cause recovery of displacement damage. The resulting microstructure was examined by cross-section TEM at 200 kV.³⁵ The TEM was performed using (001) Si because this orientation facilitated observation of cavity-wall faceting. Specimens for TEM were prepared by gluing together two implanted surfaces and then dimpling and ion-mill thinning the structure perpendicular to the interface.

Temperature-ramp experiments were performed in an ion-scattering chamber evacuated by a turbomolecular pump to a pressure of about $3 \times 10^{-5} \text{ Pa}$. This chamber was connected to an ion-implantation accelerator for the injection of H and also to a Van de Graaff accelerator for nuclear-reaction analysis. We employed the deuterium isotope (D), which was depth profiled using the ^3He -induced reaction $\text{D}(^3\text{He}, p)^4\text{He}$; emitted protons were

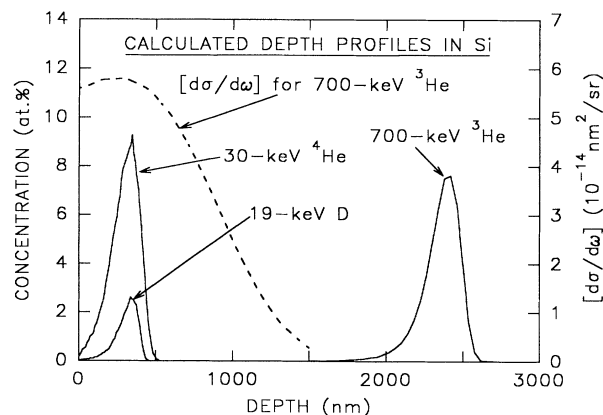


FIG. 3. Calculated depth profiles relevant to the temperature-ramp experiments. The implantation distributions are from the TRIM-90 range code (Ref. 34) while the depth-dependent differential cross section of the $\text{D}(^3\text{He}, p)^4\text{He}$ reaction was obtained using the energy-dependent cross section (Ref. 38) and the stopping power for He in Si.³⁹

counted by a Si surface-barrier detector subtending a solid angle of 0.078 sr centered at a scattering angle of 150°. A stainless-steel sheet of thickness 0.25 mm between the specimen and the detector ranged out all charged particles except the 13-MeV protons from the $^3\text{He-D}$ reaction.

Since the temperature ramps extended to 1075 K, it was important to achieve good thermal contact between the thermocouple temperature sensor and the Si specimen. To this end we welded a chromel-alumel thermocouple bead to a Mo plate and then formed a reaction bond between the Mo plate and the back of the Si. The bond was formed by introducing a 15- μm foil of Al between the Si and the Mo and raising the temperature to 973 K for 30 min. Aluminum melts at 934 K, and its affinity for oxygen is sufficient to reduce the native oxides on Si and Mo. Moreover, Al in the presence of excess Si and Mo forms intermetallics that remain solid above the temperatures of the present experiments.³⁶ An important further point is that the diffusion distance for Al in Si under the annealing conditions of these experiments, as estimated using the reported diffusion coefficient,³⁷ was always less than 1 μm while the thickness of the specimen was 250 μm . Hence the Al did not diffuse to the opposite near-surface region where the D reactions of interest took place.

After the above bonding procedure, deuterium (D) was ion implanted at room temperature and an energy of 19 keV; this energy produces overlap of the D and ^4He implantation profiles, as seen from the TRIM calculations in Fig. 3. The specimen was then temperature ramped upward at 2 K/min, and periodically, without interrupting the ramp, nuclear-reaction analysis was used to determine the depth-integrated areal density of D remaining within the near-surface He-implanted layer. The analysis was performed using a ^3He energy of 700 keV so that the broad energy peak in the nuclear cross section remained near its maximum as the particles traversed the implanted region, as seen in Fig. 3. Here the depth-dependent cross section was calculated using the known energy dependence of the cross section³⁸ and the stopping power for He in Si.³⁹ In a typical analysis, 6 μC of $^3\text{He}^+$ impinged onto a sample containing 100 D/nm² during a time interval of 2 min, and the particle detector counted about 1700 protons.

The full depth profile of the D was obtained by measuring the proton yield from the nuclear reaction as a function of incident ^3He energy in the range 300–1800 keV. Such analysis required substantially more time than the single-energy measurement used to determine integrated areal density, and consequently it was necessary to freeze the D depth distribution by halting the temperature ramp and cooling the sample to room temperature. The desired depth profile $C(x)$ was extracted from the energy-dependent nuclear-reaction yield $Y(E)$ by a deconvolution procedure described elsewhere.⁴⁰

In a few instances D was introduced by heating the Si sample in D_2 gas at 873 K for 48 h. This treatment was performed in a quartz furnace tube connected to an ion-pumped vacuum system that included facilities for gas handling. Exposures began by evacuating the sample-

containing tube at room temperature to a pressure of about 3×10^{-5} Pa (2×10^{-7} Torr). A previously temperature-stabilized furnace was then moved to enclose the sample, and D_2 gas was introduced to a pressure of 87 kPa (650 Torr). The exposure was terminated by pumping out the D_2 gas with the specimen still at 873 K, and an additional 30-min vacuum anneal at the same temperature followed to remove D that was not strongly bonded to the material. Samples charged in this fashion were not subjected to temperature ramping, since the previously discussed bonding step would have caused D release. They were instead used in separate, furnace-anneal experiments to examine the influence of the method of injection on D behavior.

Infrared spectroscopy of the Si-H local stretching mode was used to observe the bonding states of the H. Multiple-internal-reflection plates were treated on both sides, and the IR absorption spectrum was measured at room temperature with a wave-number resolution of 4 cm^{-1} . Most of these experiments were carried out using the ^1H isotope rather than D because the Si- ^1H peaks have larger amplitude and are more removed from lattice phonon absorptions. Some measurements were performed using D, however, and the isotopic shift served to verify the identification of H-related absorptions.

IV. RESULTS AND ANALYSIS

A. Cavity microstructure and helium retention

The microstructure of ^4He -implanted Si after 30 min at 973 K is shown in the cross-section TEM micrograph of Fig. 4(a). This image was acquired at a slight underfocus to enhance contrast of the cavities. Most of the cavities lie in the depth range 150–350 nm with peak density near 300 nm. This distribution conforms semiquantitatively to the calculated ^4He implantation profile in Fig. 3, where the average projected range is 290 nm and the root-mean-square (rms) range spread is 90 nm. The cavity walls in Fig. 4(a) exhibit (111) and some (100) facets together with curved regions. Detailed analysis of the cavity sizes and number density, with imaged-region thicknesses being determined from thickness fringes,³⁵ yielded an average diameter of ≈ 8 nm, a depth-integrated cavity areal density of 0.029 ± 0.005 nm⁻², a cavity surface area per sample surface area of 6.7 ± 1.2 , and a cavity volume per sample surface area of 11 ± 3 nm³/nm².

Post-implantation annealing was also carried out for 1 h at 1073 K in order to examine the effects of further microstructural evolution and less retention of implanted He. Figure 4(b) shows a cross-section TEM micrograph obtained after a shorter anneal of 30 min at 1073 K. The average diameter of the cavities is ≈ 12 nm, significantly greater than observed after 973 K, and the faceting is more pronounced, as seen in the inset. The (111) surface planes are larger and more numerous than (100) planes, consistent with the (111) surface having a lower free energy as we have reported elsewhere.³⁵

Since high-pressure He within the cavities could conceivably influence the interaction of H with the walls, we

used the formalism discussed in Sec. II D to estimate the amount of He that remained after the above heat treatments. In these calculations the diffusion coefficient, solubility parameters, and Van der Waals atomic volume b for He were taken from the literature,^{29,41} while the cavity volume per unit area of sample surface observed after annealing at 973 K was assumed to be distributed in depth as a Gaussian function with average depth and rms spread given by the TRIM range code. Within the approximation of the Van der Waals equation, and with the reported molecular volume of $b=0.039 \text{ nm}^3$, the observed cavity volume could accommodate a maximum He areal density of 280 nm^{-2} . Hence, the calculation was performed using this initial areal density instead of the actually implanted fluence of 1000 nm^{-2} . (The saturation density of gaseous He given by the Van der Waals equation is only semiquantitative at very elevated pressures, so that this value cannot be used to conclude that some of the implanted ^4He was not in the bubbles.)

The result of the above calculation is shown in Fig. 5 for isothermal annealing at 973 K. The retained areal

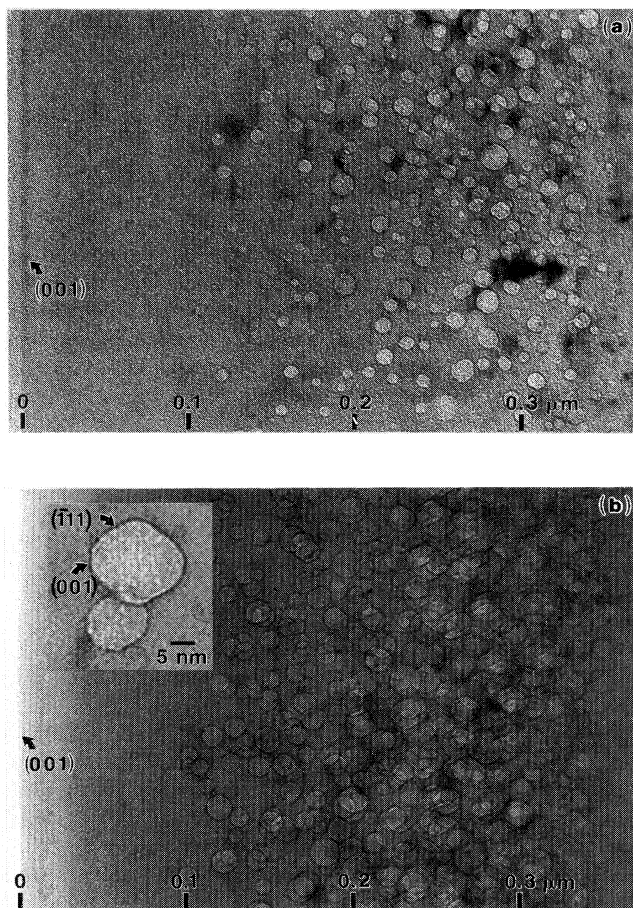


FIG. 4. Cross-section bright-field TEM micrographs of (001) Si implanted with $1000 \text{ } ^4\text{He}/\text{nm}^2$ at 30 keV and then annealed for 30 min at (a) 973 K or (b) 1073 K. The inset in (b) exhibits the faceting on an enlarged scale. The images were acquired near the (100) orientation with defocus values of -900 nm in (a), -500 nm in (b), and -200 nm in the inset.

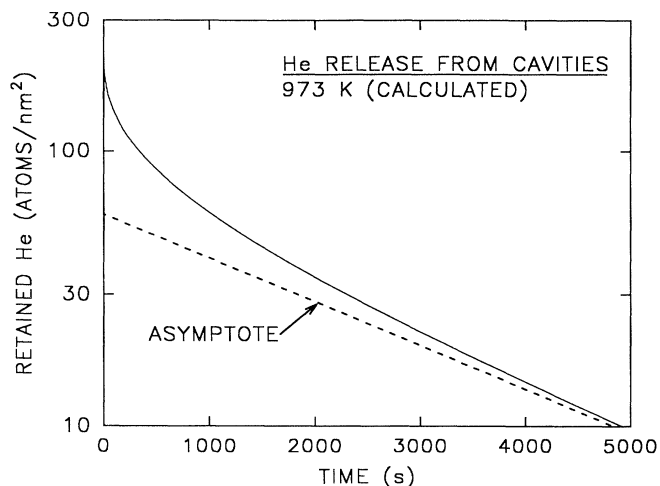


FIG. 5. Calculated release of He from cavities in Si at 973 K.

density of He is seen to decrease very rapidly at first, reflecting the nonideal behavior of the equation of state at high density, and then to approach asymptotically the exponential decay that is characteristic of an ideal gas. We believe that the formalism of Sec. II D describes the asymptotic regime quantitatively, but that the nonideal, high-density transient is given only semiquantitatively because of the limitations of the equation of state used. The treatment is nevertheless adequate to draw a key conclusion, namely that after 30 min at 973 K the He density has decreased to a few percent of its initial value and has approached the behavior of an ideal gas. Hence, He-related perturbations of the H bonded to the cavity walls are believed to be unimportant. For the 1-h anneal at 1073 K, the calculated quantity of retained He is negligible.

The accuracy of the transport formalism in describing He release from Si was tested by applying it to earlier experiments where the thermal release of ion-implanted He was measured.²⁰ In that work the implantation depth was smaller, about 30 nm, and the ramp rate much higher, 600 K/min. The complexity of nonideal-gas behavior was avoided by first forming cavities with a relatively high He fluence, then fully outgassing the He, and finally reimplanting a much smaller fluence of He before the temperature ramp. The half-amplitude point of the measured release occurred at approximately 1110 K, whereas our no-free-parameter simulation predicts 1080 K, which is satisfactory agreement.

B. Thermal release of deuterium and qualitative interpretation

Data from our temperature-ramp experiments are shown in Fig. 6. In ramp no. 1 the sample was first ion implanted with 30 keV ^4He and 700 keV ^3He , both to a fluence of 1000 nm^{-2} , and then vacuum annealed for 30 min at 973 K. Deuterium was subsequently implanted at 19 keV to a nominal fluence of 100 nm^{-2} , and the temperature was finally ramped upward at 2 K/min. The retained areal density of D was measured periodically

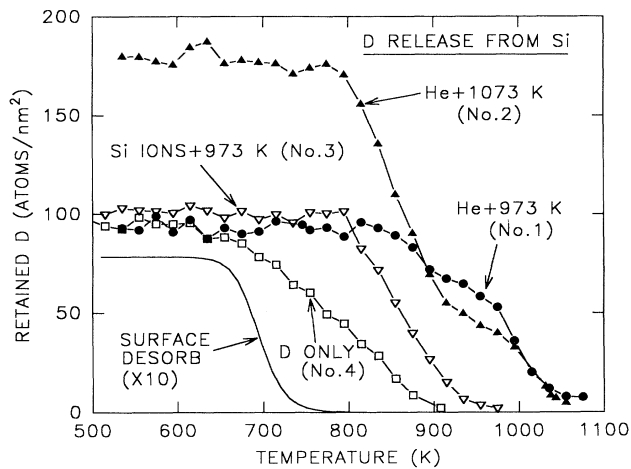


FIG. 6. Retention of ion-implanted D during temperature ramping at 2 K/min. Ramps no. 1 and no. 2 are from samples implanted with 30 keV He and then annealed at 973 or 1073 K, while ramps no. 3 and no. 4 represent specimens not implanted with 30 keV He. The solid curve shows calculated desorption from the monohydride state on (111) Si (Ref. 18).

during the ramp using nuclear-reaction analysis with 700 keV ^3He . Calculated depth profiles pertinent to this experiment are shown in Fig. 3. It is apparent that the nuclear cross section, and hence the detection of D during the temperature ramp, encompassed the near-surface layers but not the ^3He layer near 2300 nm. The purpose of the latter layer was to provide a destination for detrapped D in the event that the oxidized external surface of the Si presented a significant barrier to release. In fact, as will be discussed, no appreciable surface-barrier effects were detected in these studies.

The remaining data in Fig. 6 represent variations on the above theme. In ramp no. 4, the 30-keV ^4He implantation was omitted but not the 700-keV ^3He implantation, with other procedures being unchanged. The absence of the near-surface ^4He layer is seen to have reduced the temperatures of thermal release by about 200 K. In ramp no. 3, Si-ion bombardment before the 973-K anneal was used to simulate He displacement damage without creating cavities. (The injection of 700 keV ^3He was omitted in this case for convenience.) The self-ion irradiation was performed at an energy of 200 keV and a fluence of 90 nm^{-2} , producing a concentration and depth distribution of atomic displacements similar to that of the 30-keV ^4He implantation, based on TRIM calculations; the resulting number of atomic displacements per host atom peaks at approximately ten. Although the subsequent 973-K anneal produced extensive annealing, the self-ion bombardment is seen to have significantly enhanced D retention beyond that seen in ramp no. 4, presumably reflecting a greater number of defect traps. Nevertheless, the temperature range of D release is still well below that for the specimen containing cavities. Finally, in ramp no. 2, the 30-keV ^4He implantation was followed by a more intense vacuum anneal, 1 h at 1073 K, and the nominal fluence of implanted D was increased to 180 nm^{-2} . This experiment served to exhibit more definitively the saturation of

cavity-wall traps and also to reveal the influence of greater annealing on the number of such traps.

For comparison we have included in Fig. 6 a calculated curve showing external-surface H_2 desorption from bare Si at our ramp rate of 2 K/min. This calculation employed empirical rate equations reported elsewhere for desorption of the monohydride phase from the (111) surface.¹⁸ It is noteworthy that the desorption temperatures are much lower than those for thermal release of D from Si containing internal cavities, the difference being about 300 K. This qualitative result is necessary for the validity of our assertion in Sec. II C that the reaction path for release from internal surfaces is controlled not by desorption but rather by the promotion to solution and the subsequent bulk diffusion to the surface. Taken alone, however, it does not prove the point, since the external surfaces in the present study were oxidized, and this might reduce the desorption rate.

We now interpret the results in Fig. 6 at a mostly qualitative level, presenting additional experimental results as they become relevant. Quantitative analysis using the formalism of Sec. II D will follow in Sec. IV C. One of the most significant features of the experimental data is a high-temperature release stage near 1000 K which appears only for Si that contains cavities. We associate this stage with the thermal release of D from monohydride Si-D bonds on the internal surfaces of the cavities. In the case of the specimen that was post-implantation annealed at 973 K, the amplitude of the stage corresponds to a depth-integrated areal density of about 70 bonding sites per nm^2 of external sample surface, whereas after post-implantation annealing at 1073 K the value is about 50 nm^{-2} . Such a difference is plausible in light of the TEM micrographs in Fig. 2, which exhibit a somewhat reduced cavity-wall surface area after the higher-temperature anneal.

The absolute number of internal-surface dangling bonds available for H attachment can be semiquantitatively estimated from the observed microstructure. We do this by making use of the previously discussed observation that, after the 973-K anneal, there was approximately 7 nm^2 of depth-integrated cavity-wall surface per nm^2 of external surface. Equating the dangling-bond areal density on the wall surfaces to 7 nm^{-2} , a representative value specifically applicable to the dimerized 2×1 (100) surface and also to the unreconstructed (111) surface, one obtains approximately 50 internal surface-bonding sites per nm^2 of external surface. This agrees satisfactorily with the amplitude of the 1000-K stage, about 70 nm^{-2} .

In the case of the two specimens not implanted with 30 keV ^4He , we ascribe the observed release stages to detrapping from lattice defects. The release is seen in Fig. 6 to occur at temperatures well below the 1000-K stage associated with cavities, reflecting smaller binding energies and perhaps microstructural instability of the defects. The defects involved are unlikely to be isolated vacancies or self-interstitials in view of the elevated temperatures; possibilities include a variety of defect complexes (see, e.g., Ref. 42), perhaps stabilized to higher-than-normal temperatures by the attached H.

Ramps no. 1 and no. 2 in Fig. 6 exhibit lower-temperature stages in addition to the release at 1000 K. This results from saturation of the strong traps responsible for the 1000-K stage, leaving residual D to populate less stable states. As will be seen in Sec. IV C, these lower-temperature stages can be explained in terms of the same defect traps present in the samples without cavities. There is the additional possibility that some D_2 gas formed within the open volumes, but we will present evidence that the quantity involved is small except perhaps in the sample implanted with the relatively high D fluence of 180 nm^{-2} .

An indication of the extent of D_2 formation in the cavities of D-implanted Si was obtained by using a different method of D introduction, gas-phase charging. A useful feature of this method is that it can produce no greater D_2 pressure within the cavities than in the external gas, and under the conditions of the present experiments the resulting quantity of encapsulated D_2 is small. Therefore, if substantial D uptake is observed after gas-phase charging, it must be due primarily to Si-D bonding at cavity walls, and possibly defects, where the trapped state is lower in energy than the molecular gas. Moreover, when the fluence of ion-implanted D is not significantly greater than the observed uptake from the molecular gas, one can infer that most of the D will move to available strong trapping centers instead of forming D_2 gas.

The above charging experiment was performed on Si that had been implanted with 30 keV ^4He and then vacuum annealed at 973 K. The specimen was subsequently immersed in D_2 gas at 873 K and a pressure of 87 kPa (650 Torr) for 48 h, and finally vacuum annealed for 30 min at 873 K to remove D that was not strongly bound within the material. The permeability of D in Si at 873 K (Ref. 30) is such that in 48 h approximately 100 D/nm^2 could reach sinks at the calculated average cavity depth of 290 nm. The uptake measured by nuclear-reaction analysis was 85 D/nm^2 ; yet, by applying the ideal-gas equation of state to the observed cavity volume of 11 nm^3 per nm^2 of sample surface, one finds that the areal density of D encapsulated as D_2 gas could be no greater than 0.16 D/nm^2 . We therefore infer that most of the absorbed D was in trapped states energetically preferred over D_2 gas. Moreover, ramp no. 1 in Fig. 6 shows an areal density of 83 D/nm^2 at 875 K, virtually identical to the value from gas-phase charging. It is therefore probable that encapsulated molecular gas contributed relatively little to D retention near 875 K in the temperature ramp.

In presenting the above interpretation we emphasize that, at the temperatures of thermal release in Fig. 6, there is expected to be rapid recombinative desorption of D_2 from the cavity walls into the adjacent void. Since the cavities are not vented, however, the D_2 pressure increases until desorption is balanced by readsorption, thereby achieving local equilibrium between Si-D on the wall and D_2 in the void. The very small fraction of D in the gaseous state therefore indicates that the chemisorbed state is energetically preferred.

Infrared spectroscopy further illuminated the bound states of the H.²⁵ Measurements were performed on specimens both with and without implanted He that had

been H charged by ion implantation or by heating in H_2 gas. The ^1H isotope was employed to obtain larger signals and better isolation of the H-related spectral features. Figure 7 shows selected absorption spectra for two samples, one initially implanted with $1000 \text{ } ^4\text{He/nm}^2$ and vacuum annealed at 973 K for 30 min, and the other not implanted with He. Before the spectroscopic measurements, both of these specimens were ion implanted at room temperature with 19 keV ^1H to a fluence of 100 nm^{-2} and then subjected to isochronal anneal sequences consisting of 30-min treatments at intervals of 50 K. The horizontal axis in Fig. 7 encompasses the frequencies of Si-H stretch modes previously identified with H at displacement defects in Si.⁴³ For comparison, frequencies of two prominent surface-hydride stretch vibrations are indicated by vertical lines on the figure: the one at 2084 cm^{-1} was reported for the monohydride state on the ideally terminated (111) surface;¹ the one at 2100 cm^{-1} was observed on the H-exposed (100) surface and was ascribed to the surface monohydride, along with a second peak at 2087 cm^{-1} that in our experiments would be difficult to resolve separately from the vibration at 2084 cm^{-1} .¹² Fortunately, these surface-related peaks lie in a gap between the frequencies of defect-related structural features.

After annealing at 423 K, the IR absorption spectra from both samples exhibit numerous structures reflecting the varied environments of the Si-H bonds. In the case of the sample not implanted with He, the resolved peaks are consistent with previously reported spectra of H at displacement damage in H-implanted Si.⁴³ The specimen with He-induced cavities also exhibits these features, but in addition it shows significant absorbance in the

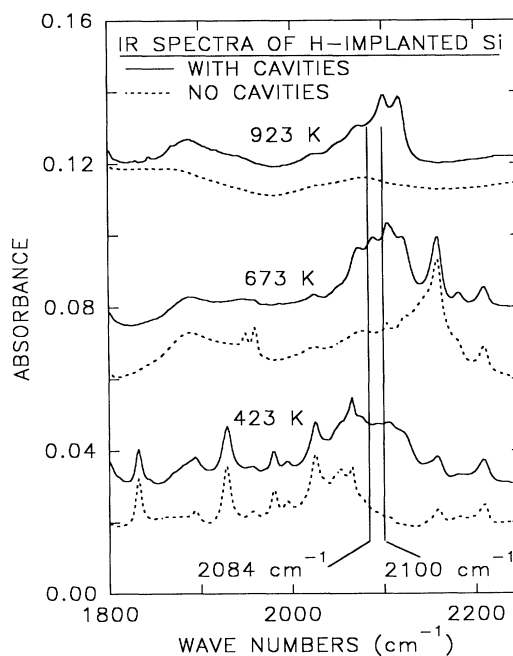


FIG. 7. Infrared absorption spectra of Si specimens with and without cavities which were ion-implanted with ^1H at room temperature and then subjected to isochronal annealing.

surface-related region near 2100 cm^{-1} . We interpret this to mean that, at lower temperatures, the implanted H associates more or less randomly with the available defects and internal surfaces. After annealing to 673 K, the spectra have changed substantially, despite the fact that Fig. 6 shows no significant decrease in the retained areal density of D at this temperature. For the sample without cavities, there is growth of some defect peaks at the expense of others, reflecting an internal redistribution of D to more stable bound configurations. Redistribution is also apparent for the Si specimen containing cavities, but here the movement is predominantly to centers with Si-H frequencies near 2100 cm^{-1} . We ascribe this to the formation of Si-H bonds on the internal surfaces of the cavities.

The specific H-defect centers responsible for the various defect peaks in Fig. 7 have not been definitively determined, and a detailed interpretation will not be attempted here. We note, however, that experimental and theoretical evidence has been used to argue that frequencies below about 2050 cm^{-1} are predominantly associated with interstitial defects while higher frequencies are mostly produced by vacancy defects (see, e.g., Ref. 44 and citations therein). Our results appear consistent with this interpretation in that cavities should be akin to vacancy defects and, in fact, the cavity-associated absorption frequencies appear above 2050 cm^{-1} . Comparison of Fig. 7 with Fig. 6 shows that most of the IR absorption has shifted to the higher frequencies before the onset of H release. Hence, assuming that the above identification criterion is valid, the defect-associated release stages in Fig. 6 mostly reflect the detachment of H from vacancy-like centers.

The uppermost pair of spectra in Fig. 7 was obtained after annealing at 923 K, a temperature above all of the release stages in Fig. 6 except the one attributed to monohydride bonding on the cavity walls. Infrared absorption in the sample not containing cavities is seen to have virtually disappeared, consistent with the nuclear-reaction data in Fig. 6. For the Si with cavities, however, there remains a pronounced absorption band encompassing the frequencies characteristic of surface monohydrides.

The sequence of IR spectra is continued to higher temperatures in Fig. 8, where the wave-number scale has been expanded and where we have included data from a specimen charged in H_2 gas at 873 K rather than H-ion implanted. When comparison is made with the temperature-ramp data in Fig. 6, it is apparent that the final stage of D release from cavity-containing Si near 1000 K corresponds to the dissociation of Si-H having stretch frequencies near 2084 and 2100 cm^{-1} . These spectral peaks decrease in unison as the temperature increases, indicating that the associated binding energies are nearly identical. Since these two frequencies have been identified with monohydrides on the (111) and (100) Si surfaces, respectively,^{1,12} this further supports our interpretation of the 1000-K temperature-ramp stage as release from monohydride states on internal surfaces. In the specimen where H was implanted, the two peaks move slightly downward in frequency between 923 and

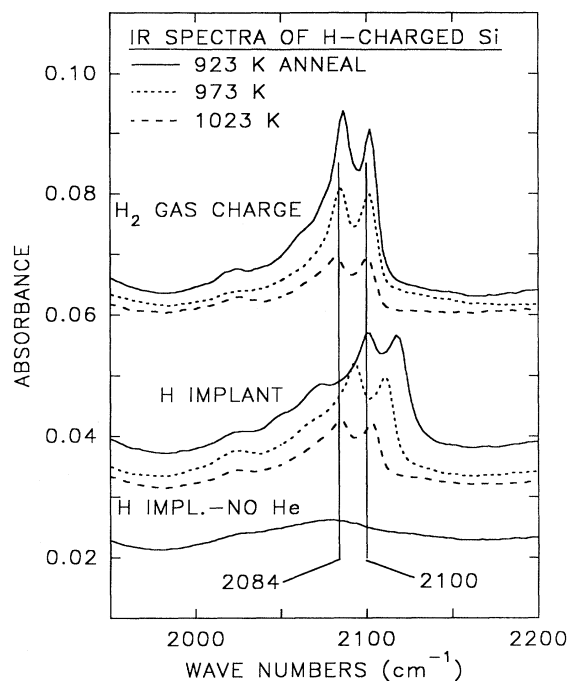


FIG. 8. Infrared absorption spectra of Si specimens with cavities which were ion implanted with ^1H at room temperature or charged in $^1\text{H}_2$ gas at 873 K and then subjected to isochronal annealing. The lowermost spectrum is from a sample without cavities.

1023 K, perhaps reflecting the annealing of residual lattice strain from the implantation.

A significant issue for quantitative interpretation of the temperature-ramp data in Fig. 6 is the degree to which the trapping centers undergo microstructural evolution during the ramp. The mathematical formalism of Sec. II D was derived assuming that the traps are static, with H undergoing repeated detrapping and retrapping during its migration through the lattice. If in reality the concentration of a particular type of trap decreases within the temperature range of observed D release from that trap, the consequent reduction in retrapping shifts the associated release stage downward in temperature relative to its calculated position. In the case of the cavity-wall traps such effects are believed to be unimportant. This is supported by the thermal stability of the cavities demonstrated in Sec. IV A. It is further reinforced by our finding in separate experiments using nuclear-reaction analysis²⁶ and IR spectroscopy²⁵ that, after the D or ^1H has undergone thermal release, the cavity-wall sites can be repopulated to the same saturation level by heating in molecular gas or in H plasmas. Defect traps within the Si lattice generally have less thermal stability in the temperature range of interest,⁴² however, so that for these entities the extraction of H binding energies using the formalism of Sec. II D may be less quantitative.

We now consider the possibility of H-barrier effects at the oxidized external surfaces of the Si samples. A sensitive way of detecting such effects is to introduce strong sinks for H at a depth beyond the layer where the H is in-

itially implanted. Then, when the temperature is sufficiently high to induce detrapping, the mobile H may either escape at the nearby surface or become attached to the sinks. If surface-barrier effects are absent altogether, the partitioning between sinks and surface is determined simply by random-walk statistics, and in the approximation of zero layer widths the two quantities of H are proportional to the respective reciprocals of the diffusion distances. If surface-barrier effects are significant, however, the fraction of H going to the internal sinks is increased. In the present studies, the buried sinks were the cavities formed by ^3He implantation at 700 keV (Fig. 3), and the population of these sinks was measured by nuclear-reaction profiling.

The above test was performed using the specimen of temperature ramp no. 4 in Fig. 6. This sample was implanted with 700 keV ^3He but not with 30 keV ^4He , so that the near-surface D-implanted layer contained only relatively weaker defect traps. As a result, the release of D from the near-surface region was complete by the end of the ramp at 908 K, well below the point where detrapping would occur from the cavity traps deeper within the specimen. The determination of the depth profile at the completion of the temperature ramp is exhibited in Figs. 9 and 10, which show, respectively, the nuclear-reaction yield as a function of energy and the D depth profile obtained by deconvolution. The deconvolution was accomplished by representing the D profile as contiguous straight-line segments and vertically adjusting the termini of these segments so that the calculated nuclear-reaction yield was fitted to the experimental reaction yield in a least-squares sense.⁴⁰ In this calculation the nuclear cross section and the stopping power for He in Si were taken from the literature.^{38,39}

The depth profile in Fig. 10 shows that most of the implanted D has moved away from the initial injection depth near 310 nm, with the areal density in the range 0–1000 nm having decreased from 98 to 3 D/nm². A significant fraction, 14 D/nm², has moved to a peak cen-

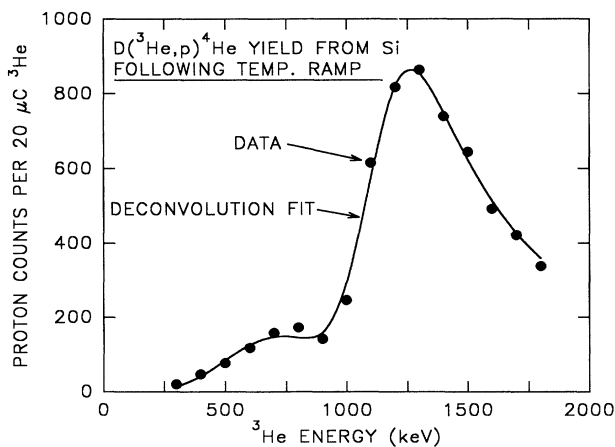


FIG. 9. Yield of nuclear-reaction protons from a Si specimen implanted with 1000 $^3\text{He}/\text{nm}^2$ at 700 keV and 98 D/nm² at 19 keV and then temperature ramped to 908 K. Each point was produced by 20 μC of incident $^3\text{He}^+$ ions. The curve represents the deconvolution fit giving the D depth profile in Fig. 10.

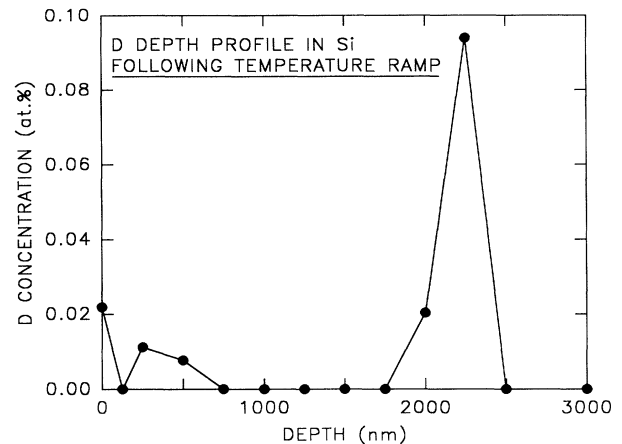


FIG. 10. Deuterium concentration-vs-depth profile obtained by deconvolution of the data in Fig. 9.

tered near 2300 nm, conforming to the calculated distribution of 700 keV ^3He shown in Fig. 3. The approximate partition rule given above predicts that, for barrier-free release, the areal density of D within the ^3He layer should be $\approx (98-3) \times (1/1990) / (1/310 + 1/1990) \approx 13 \text{ nm}^{-2}$. A more elaborate treatment, taking into account the actual distributions of the implantation depths, gives the same result to two significant figures. The observed value of 14 D/nm² is consistent with this prediction, indicating that the surface-barrier effects are not large.

C. Mathematical modeling of thermal release

The application of the transport formalism of Sec. II D to the temperature-ramp results of Fig. 6 is represented by solid curves in Fig. 11, with parameter values being summarized in Table I. Based on the presence of distinct release stages in the temperature-ramp data, the D was assumed to interact with two types of static lattice-defect

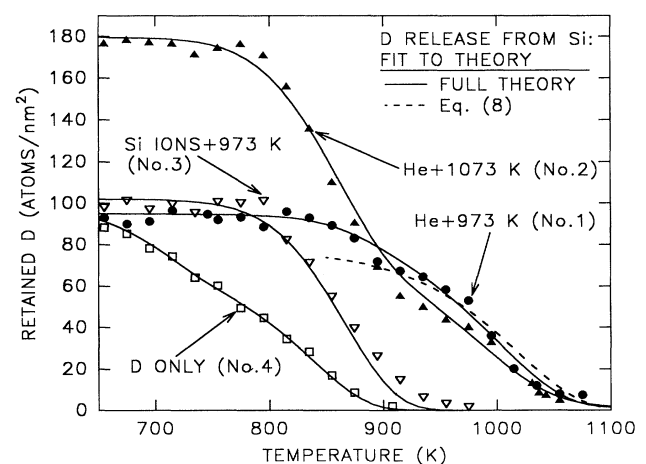


FIG. 11. Fit of diffusion-trapping theory to the temperature-ramp data. The solid curves represent the general formalism of Sec. II D, while the dashed curve was obtained by applying Eq. (8) to the cavity-wall traps.

TABLE I. Parameters used to model the temperature-ramp data in Fig. 11.

Parameter	Meaning	Value	Source
D_s	D diffusion coefficient	$6.6 \times 10^{11} \text{ nm}^2/\text{s}$ $\times \exp(-0.48 \text{ eV}/kT)$	Ref. 29
R_1	defect-trap radius	1 nm	typical value
R_2	defect-trap radius	1 nm	typical value
R_3	cavity-trap radius	4 nm	TEM after 973 K
n_1	bonding sites per defect	1	typical value
n_2	bonding sites per defect	1	typical value
n_3	bonding sites per cavity	1600	TEM after 973 K
Q_1	defect-trap binding energy	1.34 eV	fit to data
Q_2	defect-trap binding energy	1.65 eV	fit to data
Q_3	cavity-trap binding energy	2.07 eV	fit to data
$\Lambda_1 \equiv N_h \int A_1 dx$	defect-trap areal density	- - - (ramp no. 1)	not applicable
		- - - (ramp no. 2)	not applicable
		- - - (ramp no. 3)	not applicable
		40 nm^{-2} (ramp no. 4)	fit to data
Λ_2	defect-trap areal density	130 nm^{-2} (ramp no. 1)	fit to data
		130 nm^{-2} (ramp no. 2)	fit to data
		130 nm^{-2} (ramp no. 3)	fit to data
		60 nm^{-2} (ramp no. 4)	fit to data
Λ_3	cavity-trap areal density	77 nm^{-2} (ramp no. 1)	fit to data
		62 nm^{-2} (ramp no. 2)	fit to data
		- - - (ramp no. 3)	not applicable
		- - - (ramp no. 4)	not applicable

traps in Si not containing cavities, while in the presence of cavities a third type of trap was included to take account of the wall bonding sites. The diffusion coefficient of D in Si was obtained by dividing reported values for ^1H (Ref. 29) by $\sqrt{2}$ to take into account the mass difference. Barrier effects at the external surface were assumed to be negligible on the basis of the profiling results discussed at the end of the preceding subsection. The depth profile of the cavity-wall traps $A_3(x)$ in Eq. (4) was taken to be a Gaussian function having the average depth and rms spread of the implantation profile of 30 keV ^4He as calculated using the TRIM range code. The presence of the ^3He -implanted layer at 700 keV was taken into account in a similar fashion, assuming the same constant of proportionality between traps and implanted He concentration. The ^3He layer was found to have little influence on the calculated curves in Fig. 11 because of its relatively large distance from the D-implanted region. As a matter of convenience, the defect traps in the near-surface region were assigned the same depth dependence as the implanted 30-keV ^4He . The calculated temperature-ramp curves are relatively insensitive to the detailed shape of the defect profile and, furthermore, in this paper we ascribe only semiquantitative significance to the binding energies obtained for lattice-defect traps.

The values of the trap capture radius R_i and the number of binding sites per trapping center n_i have very little influence on the predicted D release after the trap concentration profile $A_i(x)$ is specified. This is so because, at the temperatures of D release, there is near equilibrium locally between the traps and adjacent solution sites, so that the expression within braces following (R_i/n_i) in Eq. (4) remains continuously near zero. In the case of the cavity traps, we equated R_i to the approximate average

radius of 4 nm observed by TEM after the post-implantation annealing at 973 K, whereas for the lattice defects a somewhat arbitrary but typical value of 1 nm was employed. The parameter n_i for the cavities was estimated from the cavity radius and the surface density of dangling bonds to be 1600, while the value for lattice defects was equated to the typical value of 1.

The remaining undetermined quantities for the model calculations are the strengths and depth-integrated areal densities of the three types of trap, and these were obtained by fitting to the temperature-ramp data. When the amount of D was sufficient to produce clear saturation of a particular type of trap, we first selected the trap areal density to reproduce the observed amplitude of the associated release stage, and then adjusted the binding energy to reproduce the observed release temperature. The calculated release temperature is approximately proportional to the sum of the trap binding energy and the diffusion activation energy, with the dependence on trap areal density being substantially weaker. Saturation is apparent for the cavity-associated traps producing the stage near 1000 K in ramps no. 1 and no. 2 of Fig. 11, and also for the stronger of the two lattice-defect traps which influence ramp no. 4. The remaining lattice-defect stages in the figure were fitted by optimally reproducing the shape and central temperature with the constraint that the already determined binding energy of the stronger lattice-defect trap was not altered, and further, that the areal density of the stronger defect traps was the same for He-implanted and Si-ion-irradiated samples. The results are summarized in Table I.

We noted in Sec. IID that the kinetics of thermal release from cavity-wall traps are, in fact, relatively simple, in part because the release stage occurs after depopu-

lation of other trapping centers. This is illustrated by applying the simplified formulation of Eq. (8), using parameters appropriate for cavity-wall traps annealed at 973 K. The trap binding energy Q_T , the areal density of traps Λ_T , and the D diffusion coefficient were taken from Table I, while the trap depth l was equated to the average implantation range of 30 keV ^3He obtained from the TRIM range code, 290 nm. The result of the calculation is given by the dashed curve in Fig. 11. The simplified treatment is seen to depart only slightly from the more elaborate calculation in the region of the 1000-K release stage. This comparison reinforces the point that the relationship between the highest-temperature release stage and the binding energy of D at the cavity walls is straightforward and provides a realistic means of quantifying the binding energy.

An interesting feature of Fig. 11 is that some of the calculated release stages are slightly broader than their experimental counterparts. This is most noticeable in ramps no. 1 and no. 2 for the stage ending near 900 K. One possible cause is the annealing out of some defect traps during the release stage, so that the extent of re-trapping progressively diminishes during the stage. This modest disparity is not believed to be important for the purposes of the present paper.

The possibility of D_2 formation within cavities was not included in the model calculations of Fig. 11. Experimental justifications for this were presented in Sec. IV B, where we showed that the fraction of D in molecular gas was small, except possibly in ramp no. 2, and further that the chemisorption on cavity walls is energetically preferred. It was nevertheless instructive to calculate the temperature-ramp release stage for D_2 initially within thermal cavities. The treatment paralleled that of He release, which was discussed in Sec. IV A, and the same cavity microstructure was assumed. The principal difference was the use of Eq. (6), which contains the square root of fugacity instead of its first power, reflecting the fact that the H_2 molecule is diatomic. The starting areal density of D atoms present as D_2 was 100 nm^{-2} , the Van der Waals molecular volume was $b = 0.044 \text{ nm}^3$,⁴¹ the solubility of H in Si was taken from the literature,²⁹ and for simplicity other trapping effects were omitted. The half-amplitude temperature of the resulting release stage was 920 K, well below the temperature of debonding from internal surfaces. This temperature does imply, however, that D_2 gas is competitive with lattice-defect traps; the reasons for its modest influence on the present temperature-ramp results are, first, that for ramps no. 3 and no. 4 the requisite open cavity volumes were not present, and second, that for ramp no. 1 there were sufficient wall-bonding sites to intercept most of the D that encountered cavities.

The theoretical fitting in Fig. 11 yields a trap binding energy for D at cavity-wall sites of $Q_3 = 2.07 \text{ eV}$ with an estimated uncertainty of $\pm 0.2 \text{ eV}$. Conversion to Si-D bond energy, which is expressed relative to the D atom in vacuum, is accomplished using Eq. (5). Taking the well established values $E_S = 1.86 \text{ eV}$ (Ref. 29) and $E_R = 4.52 \text{ eV}$, we obtain $E_B = 2.5 \pm 0.2 \text{ eV}$.

The remaining fitted binding energies, $Q_1 = 1.3 \text{ eV}$ and

$Q_2 = 1.6 \text{ eV}$, are characteristic of H trapping at defects. The fact that the corresponding Si- ^1H stretch frequencies in Fig. 7 lie above 2050 cm^{-1} suggests that the responsible defects are of vacancy type.⁴⁴ Specific structural identification is not possible from the present work, however. It should also be noted that the defect microstructures may have evolved during the release stages, in which case the assumption of static trapping centers in the model calculations would not be strictly valid. Hence, Q_1 and Q_2 should be regarded as semiquantitative.

V. DISCUSSION AND IMPLICATIONS

The Si-H surface-bond energy of $2.5 \pm 0.2 \text{ eV}$ obtained in this work is close to the dissociation energy for Si-H bonds at the (111) Si-SiO₂ interface previously derived from EPR experiments, $2.56 \pm 0.06 \text{ eV}$.²¹ The value is substantially smaller, however, than the reported dissociation energy of the $\text{H}_3\text{Si-H}$ bond in silane, 3.9 eV .²² We suggest that these relationships largely reflect the influence of the nearest-neighbor environment of the Si atom to which the H atom is attached. For both the Si surface and the (111) Si-SiO₂ interface, the subject Si atom is bonded to three Si atoms of the crystalline substrate; differences in coordination appear only at the next-nearest neighbors, some of which are oxygen in the case of the Si-SiO₂ interface. The immediate bonding environment is qualitatively different for silane, where a single Si atom forms four Si-H bonds.

The influence of nearby bonding on the Si-H bond energy is exhibited in recent theoretical work by Edwards, who employed a semiempirical molecular-orbital technique to treat the interaction of H atoms with the Si dangling orbital at the Si side of the (111) Si-SiO₂ interface.²³ His calculated energy for Si-H dissociation is 2.7 eV , in good agreement with the experimental value of 2.56 eV . Edwards has more recently used the same theoretical methods to calculate the dissociation energy for the $\text{H}_3\text{Si-H}$ bond in silane.²⁴ He obtains 3.65 eV , again in good agreement with experiment. These calculations indicate that the environment of the Si dangling orbital can indeed lead to shifts as large as 1 eV in its affinity for H.

Having obtained the strength of the Si-H surface monohydride bond, we now consider its implications for the energetics of desorption and adsorption represented in Fig. 1. Combining $E_B = 2.5 \text{ eV}$ with the average reported desorption activation energy $E_D \approx 2.5 \text{ eV}$ and the H-H recombination energy $E_D = 4.5 \text{ eV}$, we obtain from Eq. (1) the activation energy for H_2 chemisorption: $E_A \approx 2.0 \text{ eV}$. This relatively large value is consistent with the experimentally observed difficulty of chemisorbing molecular H_2 onto Si surfaces. It therefore resolves the problem, described in Sec. II B, of small E_A resulting from previously assumed larger values of the Si-H bond energy.

Knowledge of both E_B and E_D is useful in interpreting the reaction paths by which H_2 is desorbed and adsorbed on bare Si surfaces. For example, the derived large value of E_A implies a fundamental difference from the relatively well established behavior of H on most metal surfaces.

In the case of metals, the breaking of two metal-H bonds is usually concurrent with H-H formation, and the activation energy for desorption is nearly equal to the final energy minus the initial energy (see, e.g., Ref. 31). One then has $E_D \approx 2E_B - E_R$ and $E_A \approx 0$. In the case of H on Si, the similarity of the values for E_D and E_B combined with the large E_A suggest the possibility of a two-step process in which a Si-H bond is first disrupted, consuming a large fraction of the observed desorption activation energy, followed by the exothermic reaction $H + Si-H \rightarrow H_2 + Si-$. The difference from metals may arise from the strong directionality of Si-H bonding on the Si surface, as a result of which substantial energy is required to move one H atom from its equilibrium position into the proximity of another H atom. Such directionality is evidenced by the relatively large activation energy for H surface diffusion; on the (111) 7×7 surface, for example, the reported diffusion energy is about 1.5 eV.⁴⁵

Under the conditions of our experiments, the oxidized Si surface did not detectably impede H release from the underlying bulk. Since the areal density of dangling bonds available for H occupation at the Si-SiO₂ interface is small, a value of 0.03 nm^{-2} being representative for the (111) interface,²¹ it is appropriate to explore release mechanisms which might be sufficiently rapid to account for this observation. We initially examined the first-order process previously investigated in detail by EPR whereby H atoms on the dangling bonds are released into the overlying oxide, presumably undergoing exothermic recombination to form H₂ at some later time.²¹ (Molecular H₂ is both soluble and mobile in vitreous SiO₂.⁴⁶) The activation energy obtained by EPR for the dissociation of the interfacial Si-H bonds is 2.56 eV, as noted above, while the prefactor per dangling-bond site is $1.2 \times 10^{12} \text{ s}^{-1}$. When this surface-release process was incorporated into the formalism of Sec. IID in order to treat temperature ramp no. 4 in Fig. 11 and the associated depth profile in Fig. 10, agreement with the experimental data was poor. At 908 K with a dangling-bond areal density of 0.03 nm^{-2} , the model calculation showed only 0.20% of the initially implanted D fluence of 97 nm^{-2} having left the sample, with an areal density of 74 D/nm^2 occupying the ³He-implanted layer at 2400 nm. By comparison, the experimental depth profile at 908 K shows a loss of 82% and 14 D/nm^2 occupying the deep ³He layer. Even when the areal density of dangling-bond sites was increased 1000 times to 30 nm^{-2} , which is several tenths of a monolayer, surface-barrier effects were still observed in the model calculation through the sensitive partitioning of D between surface release and the ³He sinks at 2300 nm. Hence, this mechanism is unlikely to be the dominant one in accommodating D release from the underlying Si bulk.

More rapid H release through the oxidized Si surface might occur by a recombination reaction between one H atom on the dangling-bond interfacial site and a second H atom in a nearby lattice-solution site. This process would be exothermic, with the released energy per H₂ molecule being given by $E_S + E_R / 2 - E_B = 1.6 \text{ eV}$ in the notation of Eq. (5). The key unknown is the extent to which activation barriers are present in the reaction path

between initial and final states. Here we consider hypothetically the situation where such barrier effects are small. Then, the dangling-bond sites at the Si-SiO₂ interface effectively behave as sinks for H from the underlying Si matrix; in particular, when such sites are initially unoccupied, nearby H atoms in solution form Si-H bonds, whereas when Si-H is already in place, a second approaching H atom stimulates the recombination reaction producing H₂. As a result, the release process is limited simply by the diffusion of H to the interfacial dangling-bond sites. When such a process is incorporated into the formalism of Sec. II B, assuming dangling-bond sites with an areal density of 0.01 nm^{-2} and a capture radius of 1 nm, the calculated thermal evolution of the system is virtually indistinguishable from the case of unrestricted surface release. This release mechanism therefore provides a plausible but unconfirmed explanation of the experimentally observed behavior. We also do not rule out the possibility of H-H recombination at interfacial sites removed from the dangling-bond centers.

VI. SUMMARY AND CONCLUSIONS

By characterizing the interaction of H with internal surfaces in Si we have achieved the first determination of the surface monohydride bond energy; the result is $2.5 \pm 0.2 \text{ eV}$ when referenced to the H atom in vacuum. Based on the sharpness of the associated thermal release stage and the simultaneous decrease of IR absorption structures corresponding to Si-H on (111) and (100) surfaces, this bond energy is believed to be nearly invariant over the (111) and (100) facets and curved regions of the cavity walls. Such invariance suggests, not surprisingly, that the bond energy is hardly affected by interactions beyond the nearest neighbors of the Si surface atom to which the H is attached. The above bond energy is smaller than that reported for the H₃Si-H bond in silane, in accord with theoretical calculations. It is very close to the dissociation energy of the Si₃Si-H bond at the Si-SiO₂ interface, however, as expected from the similarity of local bonding configurations. The above surface bond energy implies that the state of atomic chemisorption is energetically preferred over H₂ gas, but also that there is a substantial activation barrier of about 2 eV to the chemisorption.

The present experiments also provide a semiquantitative indication of the strength of H trapping at displacement damage in Si. Two distinct defect-related stages were observed in the thermal release, and these correspond respectively to binding energies about 0.4 and 0.7 eV smaller than that at cavity-wall sites. Based on our IR spectroscopic results and earlier work on the identification of spectral features, the above binding energies are tentatively ascribed to vacancy defects.

The oxidized external surface of Si did not detectably impede the release of H from solution, even in experiments designed to be sensitive to such effects. We therefore inferred the presence of a mechanism of rapid molecular recombination at the Si-SiO₂ interface, one controlled predominantly by diffusion within the underlying Si lattice. A previously investigated process involving

thermally activated, first-order release of H atoms from Si dangling bonds at the Si-SiO₂ interface into the oxide was shown to be too slow by orders of magnitude. This led us tentatively to propose a recombination reaction between one H atom on the interfacial dangling bond and another H atom in a nearby solution site within the Si.

ACKNOWLEDGMENTS

The authors are indebted to A. H. Edwards for permission to report unpublished theoretical results. They are

pleased to acknowledge the contributions of D. M. Bishop, who carried out the ion-beam experiments and performed much of the data analysis, and of M. P. Moran, who prepared TEM specimens and obtained micrographs. J. C. Barbour and T. Klitsner made valuable comments on the manuscript. This work was performed under the auspices of the U.S. Department of Energy and funded by its Office of Basic Energy Sciences, Division of Materials Science, under Contract No. DE-AC04-76DP00789.

- ¹G. S. Higashi, Y. J. Chabal, G. W. Trucks, and K. Raghavachari, *Appl. Phys. Lett.* **56**, 656 (1990).
- ²H. Hirayama and T. Tatsumi, *Appl. Phys. Lett.* **54**, 1561 (1989).
- ³L. T. Canham, *Appl. Phys. Lett.* **57**, 1046 (1990).
- ⁴C. Tsai, K.-H. Li, J. Sarathy, S. Shih, J. C. Campbell, B. K. Hance, and J. M. White, *Appl. Phys. Lett.* **59**, 2814 (1991).
- ⁵S. M. Prokes, O. J. Glembocski, V. M. Bermudez, R. Kaplan, L. E. Friedersdorf, and P. C. Searson, in *Light Emission from Silicon*, edited by S. S. Iyer, R. T. Collins, and L. T. Canham, MRS Symposia Proceedings No. 256 (Materials Research Society, Pittsburgh, 1992), p. 107.
- ⁶P. M. Garone, J. C. Sturm, P. V. Schwartz, S. A. Schwarz, and B. J. Wilkens, *Appl. Phys. Lett.* **56**, 1275 (1990).
- ⁷S. H. Wolf, S. Wagner, J. C. Bean, R. Hull, and J. M. Gibson, *Appl. Phys. Lett.* **55**, 2017 (1989).
- ⁸J. J. Boland, *Phys. Rev. Lett.* **65**, 3325 (1990).
- ⁹J. J. Boland, *Surf. Sci.* **244**, 1 (1991).
- ¹⁰K. Mortensen, D. M. Chen, P. J. Bedrossian, J. A. Golovchenko, and F. Besenbacher, *Phys. Rev.* **43**, 1816 (1991).
- ¹¹Y. J. Chabal, G. S. Higashi, and S. B. Christman, *Phys. Rev. B* **28**, 4472 (1983).
- ¹²Y. J. Chabal, *Surf. Sci.* **168**, 594 (1986).
- ¹³U. Jansson and K. J. Uram, *J. Chem. Phys.* **91**, 7978 (1989).
- ¹⁴G. Schulze and M. Henzler, *Surf. Sci.* **124**, 336 (1983).
- ¹⁵B. G. Koehler, C. H. Mak, D. A. Arthur, P. A. Coon, and S. M. George, *J. Chem. Phys.* **89**, 1709 (1988).
- ¹⁶P. Gupta, V. L. Colvin, and S. M. George, *Phys. Rev. B* **37**, 8234 (1988).
- ¹⁷K. Sinniah, M. G. Sherman, L. B. Lewis, W. H. Weinberg, J. T. Yates, Jr., and K. C. Janda, *J. Chem. Phys.* **92**, 5700 (1990).
- ¹⁸M. L. Wise, B. G. Koehler, P. Gupta, P. A. Coon, and S. M. George, *Surf. Sci.* **258**, 166 (1991).
- ¹⁹G. A. Reider, U. Höfer, and T. F. Heinz, *J. Chem. Phys.* **94**, 4080 (1991).
- ²⁰C. C. Griffioen, J. H. Evans, P. C. De Jong, and A. Van Veen, *Nucl. Instrum. Meth. B* **27**, 417 (1987).
- ²¹K. L. Brower and S. M. Myers, *Appl. Phys. Lett.* **57**, 162 (1990); K. L. Brower, *Phys. Rev. B* **42**, 3444 (1990).
- ²²R. Walsh, *Acc. Chem. Res.* **14**, 246 (1981).
- ²³A. H. Edwards, *Phys. Rev. B* **44**, 1832 (1991).
- ²⁴A. H. Edwards (private communication).
- ²⁵H. J. Stein, S. M. Myers, and D. M. Follstaedt, *J. Appl. Phys.* **73**, 2755 (1993).
- ²⁶W. R. Wampler, D. M. Follstaedt, and S. M. Myers, *Phys. Rev. B* (to be published).
- ²⁷S. M. Myers, D. M. Follstaedt, H. J. Stein, and W. R. Wampler, *Phys. Rev. B* **45**, 3914 (1992).
- ²⁸T. Klitsner and J. S. Nelson, *Phys. Rev. Lett.* **67**, 3800 (1991).
- ²⁹A. Van Wieringen and N. Warmoltz, *Physica* **22**, 849 (1956).
- ³⁰S. M. Meyers, G. A. Brown, A. G. Revesz, and H. L. Hughes, *J. Appl. Phys.* **73**, 2196 (1993).
- ³¹S. M. Myers, P. M. Richards, W. R. Wampler, and F. Besenbacher, *J. Nucl. Mater.* **165**, 9 (1989).
- ³²P. M. Richards, *J. Chem. Phys.* **85**, 3520 (1986).
- ³³E. A. Guggenheim, *Thermodynamics* (North-Holland, Amsterdam, 1950), pp. 98 and 99.
- ³⁴J. F. Ziegler, J. P. Biersack, and U. Littmark, *The Stopping and Range of Ions in Solids* (Pergamon, New York, 1985); J. F. Ziegler (private communication).
- ³⁵D. M. Follstaedt, S. M. Myers, W. R. Wampler, and H. J. Stein, in *Proceedings of The 50th Annual Meeting of The Electron Microscopy Society of America*, edited by G. W. Bailey, J. Bentley, and J. A. Small (San Francisco Press, San Francisco, 1992), pp. 334 and 335.
- ³⁶*Binary Alloy Phase Diagrams*, edited by T. B. Massalski, J. L. Murray, L. H. Bennett, and H. Baker (American Society for Metals, Metals Park, OH, 1986).
- ³⁷H. F. Wolf, *Semiconductors* (Wiley-Interscience, New York, 1971), p. 153.
- ³⁸W. Möller and F. Besenbacher, *Nucl. Instrum. Meth.* **168**, 111 (1980).
- ³⁹J. F. Ziegler, *Helium Stopping Powers and Ranges in All Elements* (Pergamon, New York, 1977).
- ⁴⁰S. M. Myers, G. R. Caskey, Jr., D. E. Rawl, Jr., and R. D. Sisson, Jr., *Metall. Trans. A* **14**, 2261 (1983).
- ⁴¹*CRC Handbook of Chemistry and Physics*, edited by R. C. Weast and M. J. Astle (CRC, Boca Raton, Florida, 1980), p. D-194.
- ⁴²S. J. Pearton, J. W. Corbett, and M. Stavola, *Hydrogen in Crystalline Semiconductors* (Springer-Verlag, Berlin, 1992), pp. 178–181.
- ⁴³H. J. Stein, *J. Electron. Mater.* **4**, 159 (1975).
- ⁴⁴J. W. Corbett, P. Deák, U. V. Desnica, and S. J. Pearton, in *Hydrogen in Semiconductors*, edited by J. I. Pankove and N. M. Johnson (Academic, Boston, 1991), pp. 58–61.
- ⁴⁵G. A. Reider, U. Höfer, and T. F. Heinz, *Phys. Rev. Lett.* **66**, 1994 (1991).
- ⁴⁶J. E. Shelby, *J. Appl. Phys.* **48**, 3387 (1977).

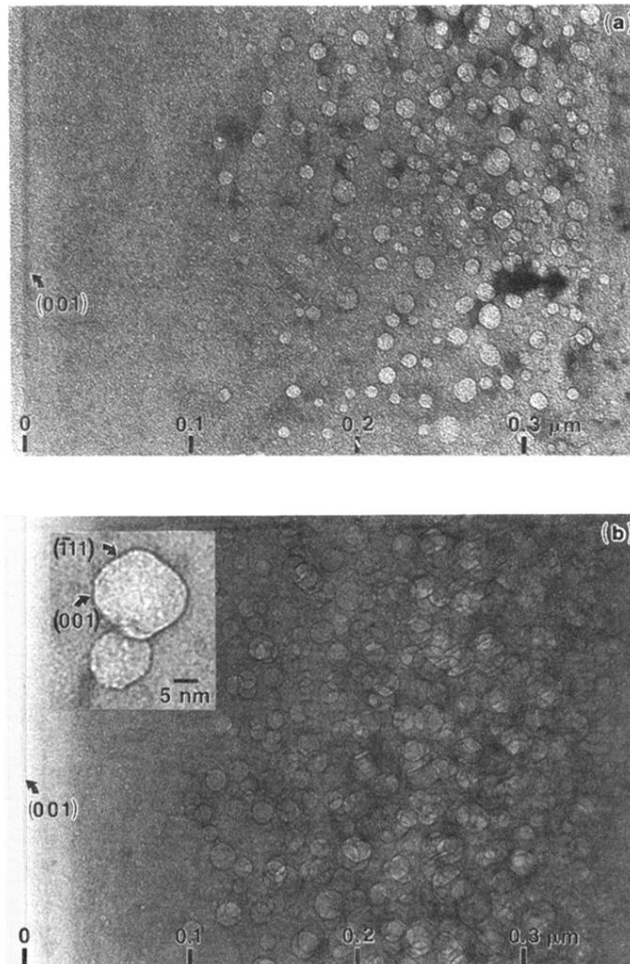


FIG. 4. Cross-section bright-field TEM micrographs of (001) Si implanted with 1000 He/nm^2 at 30 keV and then annealed for 30 min at (a) 973 K or (b) 1073 K. The inset in (b) exhibits the faceting on an enlarged scale. The images were acquired near the (100) orientation with defocus values of -900 nm in (a), -500 nm in (b), and -200 nm in the inset.